Pulsed $^{1,2}H$ ENDOR and ^{2}H–^{2}H TRIPLE Resonance of H-Bonds and Cysteinyl β-CH_2 of the *D. gigas* Hydrogenase [3Fe–4S]$^{+}$ Cluster

Peter E. Doan, Chaoliang Fan, and Brian M. Hoffman*

Contribution from the Department of Chemistry, Northwestern University, Evanston, Ilinois 60208

Received August 12, 1993®

Abstract: This paper presents the results of ^{2}H Mims and ^{1}H Davies pulsed ENDOR of the [3Fe–4S]$^{+}$ cluster of *Desulfovibrio gigas* hydrogenase. It also describes the first ^{2}H Mims pulsed TRIPLE-resonance experiments, on the exchangeable deuterons. The ^{1}H ENDOR data show that the *intrinsic* isotropic hyperfine couplings for the β-CH_2 protons of the three cysteines bound to iron fall in the range $1.3 \lesssim a \lesssim 1.9$ MHz. These values, which often had been estimated at $a = 1$ MHz, will allow better interpretation of solution NMR data for paramagnetic [*n*Fe–*m*S] clusters. The spectra show well-resolved signals from three strong NH···S H-bonds to the cluster. Mims ^{2}H–^{2}H TRIPLE-resonance has been used to assign the exchangeable deuterons and to obtain relative signs of the $^{1,2}H$ hyperfine couplings. Analysis of the hyperfine interactions in terms of spin-coupling among the three Fe(III) ions of the cluster, along with examination of the X-ray structures of several [3Fe–4S]$^{+}$ clusters, gives an intrinsic hyperfine coupling of $a(^{1}H) \sim$ 3–4 MHz for each of the three strong H-bonds and actually allows us to propose the distribution of H-bonds among the seven sulfur atoms within the $[Fe_3S_4(Cys)_3]^{2-}$ center.

Introduction

We recently discovered[1] that Mims pulsed electron-nuclear double-resonance (ENDOR) spectroscopy[2,3] gives extremely well-resolved ^{2}H ENDOR spectra and provides significant new opportunities for studying both hydrogen bonding[4] and exogenous ligands to [*m*Fe–*n*S] clusters. We now have extended this observation and report the use of ^{1}H Davies pulsed ENDOR[5] and ^{2}H Mims ENDOR to study separately the intricate resonance patterns from constitutive cysteinyl β-CH_2 protons as well as from exchangeable H-bonded protons of the [3Fe–4S]$^{+}$ cluster of *Desulfovibrio (D.) gigas* hydrogenase. We further report the first ^{2}H Mims pulsed TRIPLE-resonance[5] experiments on the exchangeable deuterons.

The [3Fe–4S]$^{+}$ clusters in principle provide a good test case for such studies because all three iron ions have a well-defined Fe(III) valency. However, their EPR spectra typically cannot be described by a well-defined **g** tensor, but rather appear to exhibit a distribution in tensor values that reflects a distribution in structure,[6] and this limits the amount of data available from ENDOR. This limitation is substantially relaxed for the [3Fe–4S]$^{+}$ cluster of *D. gigas* hydrogenase, making it an excellent vehicle for the present investigation. EPR and ^{57}Fe ENDOR measurements[7] show that the major form of the protein, which is the primary focus of this study and is here denoted as form 1, is present to ~70%, and its cluster has a well-defined **g** tensor that reflects a well-defined structure. The minority form, denoted form 2, has a more plastic structure, as reflected in a significant distribution in **g** tensor values, but its ENDOR signals can largely be distinguished from those of form 1.

The $^{1,2}H$ pulsed ENDOR data for both cluster forms show well-resolved signals from three strong NH···S hydrogen bonds, and the spectra for form 1 show the field dependencies (orientation selection)[8–10] necessary for detailed analyses. In contrast, although electron spin echo modulation (ESEEM)[11] and continuous wave (CW) ENDOR[12,13] studies show that this [3Fe–4S]$^{+}$ cluster is susceptible to H/D exchange, neither method is able to characterize the exchangeable protonic species. The first Mims ^{2}H–^{2}H TRIPLE-resonance[2,3,5] has been used to assign the exchangeable deuterons to an individual cluster form and to obtain relative signs of the $^{1,2}H$ hyperfine couplings. Analysis of the hyperfine interactions in terms of spin coupling among the three Fe(III) ions of the cluster, along with examination of the X-ray structures of several [3Fe–4S]$^{+}$ clusters,[14–16] actually allows us to propose the distribution of the three strongly-coupled H-bonds among the seven sulfur atoms bonded to Fe. The data reported here suggest that pulsed $^{1,2}H$ ENDOR and solution NMR will play complementary roles in studying chemically significant H-bonds[17,18] to Fe–S clusters. As an additional feature of this study we obtain hyperfine coupling constants for the cysteinyl β-CH_2

* Abstract published in *Advance ACS Abstracts,* December 15, 1993.

(1) Fan, C.; Kennedy, M. C.; Beinert, H.; Hoffman, B. M. *J. Am. Chem. Soc.* **1992**, *114*, 374–375.
(2) Mims, W. B. *Proc. R. Soc. London, A* **1965**, *283*, 452–457.
(3) Gemperle, C.; Schweiger, A. *Chem. Rev.* **1991**, *91* (7), 1481–1505.
(4) Rypniewski, W. R.; Breiter, D. R.; Benning, M. M.; Wesenberg, G.; Oh, B.-H.; Markley, J. L.; Rayment, I.; Holden, H. M. *Biochemistry* **1991**, *30*, 4126–4131.
(5) Grupp, A.; Mehring, M. In *Modern Pulsed and Continuous-Wave Electron Spin Resonance*; Kevan, L.; Bowman, M. K., Eds.; John Wiley & Sons: New York, Chichester, Brisbane, Toronto, Singapore, 1990; Chapter 4, pp 195–229.
(6) Guigliarelli, B.; More, C.; Bertrand, P.; Gayda, J. P. *J. Chem. Phys.* **1986**, *85* (5), 2774–2778.
(7) Fan, C.; Houseman, A. L. P.; Doan, P.; Hoffman, B. M. *J. Phys. Chem.* **1993**, *97*, 3017–3022.
(8) Hoffman, B. M. *Acc. Chem. Res.* **1991**, *24* (6), 164–170.
(9) Hoffman, B. M.; DeRose, V. J.; Doan, P. E.; Gurbiel, R. J.; Houseman, A. L. P.; Telser, J. In *Biological Magnetic Resonance*; Berliner, L., Ed.; Plenum Press: New York, 1993.
(10) Doan, P. E.; Hoffman, B. M. Manuscript in preparation.
(11) Mims, W. B.; Peisach, J. In *Advanced EPR. Applications in Biology and Biochemistry*; Hoff, A. J., Ed.; Elsevier: Amsterdam–Oxford–New York–Tokyo, 1989; Chapter 1, pp 1–57.
(12) Fan, C.; Teixeira, M.; Moura, J.; Moura, I.; Huynh, Bol-H.; le Gall, J.; Peck, H. D., Jr.; Hoffman, B. M. *J. Am. Chem. Soc.* **1991**, *113* (1), 20–24.
(13) Unpublished 35-GHz CW-ENDOR data.
(14) Stout, C. D. *J. Mol. Biol.* **1989**, *205*, 545–555.
(15) Kissinger, C. R.; Sieker, L. C.; Adman, E. T.; Jensen, L. H. *J. Mol. Biol.* **1991**, *219*, 693–715.
(16) Merritt, E. A.; Stout, G. H.; Turley, S.; Sieker, L. C.; Jensen, L. H. *Acta Crystallogr.* **1993**, *D49*, 272–281.
(17) Adman, E.; Watenpaugh, K. D.; Jensen, L. H. *Proc. Natl. Acad. Sci. U.S.A.* **1975**, *72* (12), 4854–4858.
(18) Backes, G.; Mino, Y.; Loehr, T. M.; Meyer, T. E.; Cusanovich, M. A.; Sweeney, W. V.; Adman, E. T.; Sanders-Loehr, J. *J. Am. Chem. Soc.* **1991**, *113*, 2055–2064.

0002-7863/94/1516-1033$04.50/0

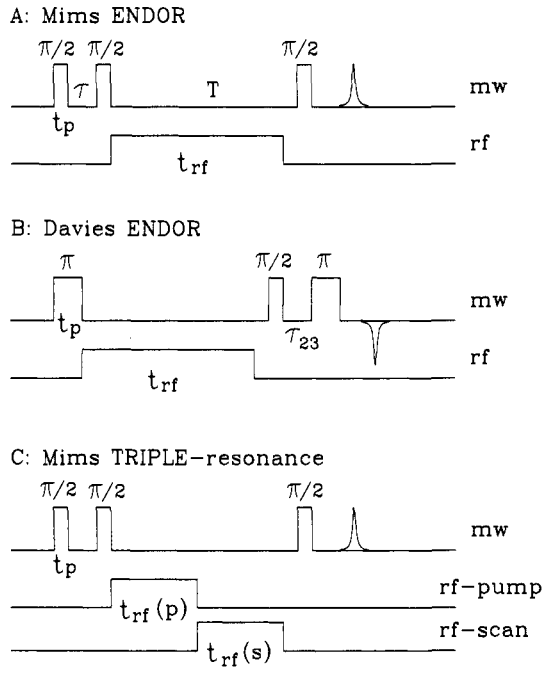

Figure 1. Pulse sequences for (A) Mims and (B) Davies pulsed ENDOR and for (C) Mims ^2H–^2H pulsed TRIPLE.

protons. This is the first analysis of the ENDOR signals from the constitutive protons of ligands to a protein-bound cluster and is relevant for the use of solution NMR measurements to determine spin-coupling parameters for [nFe–mS] clusters.[19-21]

Materials and Methods

The as-purified *D. gigas* hydrogenase samples in H_2O (denoted 3Fe–H) and D_2O (3Fe–D) solvent were prepared as previously described.[22] Pulsed EPR, ENDOR, and TRIPLE-resonance spectra were obtained on a locally-built spectrometer[23] operating at X-band (9 GHz) microwave frequency.

Mims ENDOR[2] employs a pulse sequence that consists of three $\pi/2$ microwave pulses (Figure 1A), which produce a stimulated spin echo. An rf pulse is inserted between pulses 2 and 3. The ENDOR response consists of a change in the spin-echo amplitude when the rf matches a nuclear resonance frequency. A widely perceived disadvantage of conventional Mims ENDOR (in which $t_p \ll \tau_{12}$) is that it has "blind spots" for hyperfine couplings when A (MHz) = $n/\tau_{1,2}$ (μs), n = 1,2, ... However, this limitation is not relevant for small couplings, $A < 1/\tau_{1,2}$. For example, with a typical value of $\tau_{1,2} \approx 200$ ns, a nucleus with $A < 5$ MHz can be detected without the interference of blind spots. Normally, this case applies for ^2H ENDOR.

The "blind spots"[3,24] in Mims ENDOR would interfere in the proton ENDOR, where $A \lesssim$ 8–10 MHz. Therefore, the Davies ENDOR sequence was used for proton pulsed ENDOR experiments. Here a microwave π pulse first inverts an electron spin transition (Figure 1B). An rf π pulse is then applied to the appropriate nuclear transition to induce sublevel polarization transfer. The final spin polarization is monitored by the spin echo intensity generated in a subsequent two-pulse ($\pi/2 - \pi$) detection sequence. The Davies ENDOR response, the rf-induced change in echo amplitude when the rf matches a nuclear transition, is jointly dependent on the hyperfine coupling constant, $A(n)$, and the width of the preparation pulse t_p. Nuclei with $A(n) \ll 1/t_p$ cannot be detected effectively, and the sensitivity is maximized for $A(n)t_p \sim 0.7$.[23,25,26] Therefore it is quite useful for ^1H ENDOR measurements, where couplings are large. For example when t_p = 70 ns, sensitivity is maximized for $A^n \approx 10$ MHz. It is not suitable for the ^2H ENDOR experiments. For example, $A(^2H) \approx 0.7$ MHz would require $t_p \sim 1$ μs to give a maximum fractional ENDOR response, but the initial echo intensity would be too low to be useful at this t_p.[23]

The ^2H–^2H TRIPLE-resonance[5] experiments reported here were carried out using the Mims ENDOR sequence (Figure 1C). Two rf pulses are inserted between pulses 2 and 3 of a three pulse sequence. The first rf pulse has fixed frequency and "pumps" a selected ENDOR line, while the second rf pulse is swept through the entire ENDOR spectrum. There is no time delay between the pump and probe pulses in the experiments reported here. Difference TRIPLE spectra were recorded as the [pump on – pump off] difference in ENDOR intensities. The rf power level was set to avoid interference from harmonics of ^1H resonances. The rf pulse width in ^2H ENDOR and TRIPLE-resonance experiments was determined by transient-nutation experiments[5] for maximum ENDOR and TRIPLE responses.

This paper employs several ways to discuss the intensity of a pulsed ENDOR spectrum. (i) The *absolute* ENDOR effect is simply the change in echo height (e.g. in millivolts or microwatts) for a given applied radio frequency. It is useful in comparing spectra taken from a single sample (say at different fields) for a fixed spectrometer configuration and pulse sequence. (ii) The *relative* ENDOR effect is the absolute effect divided by the echo height in the absence of rf for Mims ENDOR or in the absence of the preparation π pulse for Davies ENDOR. It is necessary to use the latter in comparing the ENDOR response of different samples studied under fixed spectrometer conditions. Thus, the ^1H spectra of exchangeable protons, below termed $\Delta(^1H)$, are taken by subtracting the *relative* ENDOR spectra of the 3Fe–D sample from the corresponding spectra from 3Fe–H. The validity of this procedure was confirmed by comparing the $\Delta(^1H)$ spectra with ^2H spectra of the deuterons introduced by the H/D exchange.

The ENDOR transition frequencies[27] for a nucleus of spin I are given to first order by the equation

$$\nu_{\pm} = |\nu(n) \pm A(n)/2 + (3P(n)/2)(2m - 1)| \qquad (1)$$

where $-I + 1 \lesssim m \lesssim I$, $A(n)$ and $P(n)$ are the orientation dependent hyperfine and quadrupole coupling constants, and $\nu(n) = g_n\beta_n B_0/h$ is the nuclear Larmor frequency. For protons (I = 1/2) and deuterons (I = 1) in biological systems, usually $\nu(n) > A(n)/2$ and the ENDOR spectrum is a hyperfine-split doublet that is split by $A(n)$ and centered about the nuclear Larmor frequency ($\nu(^1H)$ = 14.90 MHz and $\nu(^2H)$ = 2.28 MHz at B_0 = 0.3500 T). For the ^2H ENDOR, the $\nu_{\pm}$ lines are further split by the quadrupole term whose maximal value is $P(^2H) = e^2qQ/2h$. The magnetic parameters of exchangeable proton and deuteron nuclei are related by fundamental nuclear properties

$$A(^1H)/A(^2H) = \nu(^1H)/\nu(^2H) = g_H/g_D = 6.514 \qquad (2)$$

so the magnetic parameters obtained from the resonances for one isotopic species can be used to predict those of the other.

We have described in detail how ENDOR spectra from a frozen-solution sample recorded at multiple fixed fields can be used to deduce a nuclear hyperfine interaction *tensor*.[8,10] These procedures are employed here.

The EPR and ENDOR spectra reported here were taken in spectrometers operating at different microwave frequencies. Thus, we must compare spectra by referring to g value rather than field. Because the g anisotropy is small, the g values must be specified to four decimal places in order to distinguish field positions adequately. Earlier we reported $g_2 \approx 2.024$, so it is convenient to *define* $g_2 \equiv 2.0240$ and report all observed g values with respect to g_2. We emphasize that the sharpness of the EPR spectrum does not warrant this precision. However, the precision of the field (~1 part in 10^4) and frequency (stable to ~1 part in 10^5) allows us to specify $\delta g = g_{obs} - g_2$ to five significant figures.

Results and Discussion

Decomposition of the EPR Spectrum and the Consequences for Pulsed Endor. We begin by considering the EPR spectrum of the

(19) Dunham, R.; Palmer, G.; Sands, R. H.; Bearden, A. J. *Biochim. Biophys. Acta* **1971**, *253*, 373–384.
(20) Banci, L.; Bertini, I.; Luchinat, C. *Struct. Bonding (Berlin)* **1990**, *72*, 113–136.
(21) Macedo, A. L.; Moura, I.; Moura, J. J. G.; Le Gall, J.; Huynh, B. H. *Inorg. Chem.* **1993**, *32*, 1101–1105.
(22) Huynh, B. H.; Patil, D. S.; Moura, I.; Teixeira, M.; Moura, J. J. G.; DerVartanian, D. V.; Czechowski, M. H.; Prickril, B. C.; Peck, H. D., Jr.; LeGall, J. *J. Biol. Chem.* **1987**, *262* (2), 795–800.
(23) Fan, C.; Doan, P. E.; Davoust, C. E.; Hoffman, B. M. *J. Magn. Reson.* **1992**, *98*, 62–72.
(24) Davies, E. R. *Phys. Lett.* **1974**, *47A* (1), 1–2.
(25) Doan, P. E.; Fan, C.; Davoust, C. E.; Hoffman, B. M. *J. Magn. Reson.* **1991**, *95*, 196–200.
(26) Hofer, P. Ph.D. Dissertation, Stuttgart, 1988.
(27) Hoffman, B. M.; Gurbiel, R. J.; Werst, M. M.; Sivaraja, M. In *Advanced EPR. Applications in Biology and Biochemistry*; Hoff, A. J., Ed.; Elsevier: Amsterdam, 1989; Chapter 15, pp 541–591.

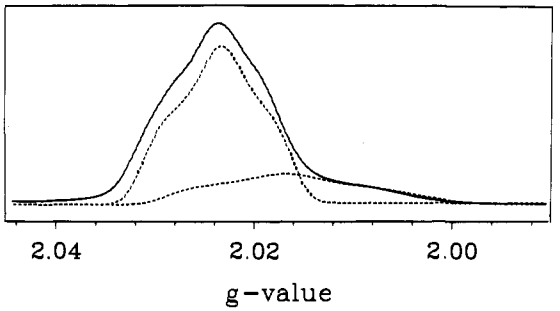

Figure 2. CW EPR spectrum (35 GHz) of the [3Fe–4S]+ cluster of *D. gigas* hydrogenase. The 100-kHz field-modulated dispersion-mode spectrum corresponds to the absorption envelope. Dashed line is the decomposition into contributions from form 1 (g(1) = [2.032, 2.024, 2.016]; 70%) and form 2 (g(2) = [2.029, 2.017, 2.003]; 30%). Conditions: ν = 35.4 GHz, mod amp ~ 1.6 G, T = 2 K.

[3Fe–4S]+ cluster of the hydrogenase and its relation to the ENDOR experiment. We have shown that the spectrum can be decomposed, as seen in Figure 2, into a contribution from a majority species (≳70%), form 1, with **g** tensor **g**(1) = [2.032, 2.024, 2.016], and a minority species, form 2, with **g**(2) = [2.029, 2.017, 2.003].[7] In addition, at the lowest fields used for ENDOR measurements ($g \gtrsim 2.02$), the spin echo height includes a 10–15% contribution from a Ni(III) center (Ni-A) thought to be the enzyme active site.[12,22,28] However, experiments at still lower field, where there is no EPR intensity from the [3Fe–4S]+ cluster and the intensity of Ni-A is greater, confirm that Ni-A makes *no* significant contribution to the pulsed ENDOR measurements reported here.

To a first approximation the absolute intensity of the pulsed ENDOR signal from a given nucleus (or nuclei), with a particular hyperfine coupling, should be proportional to the EPR signal strength of the paramagnetic center involved. For a single species with an anisotropic **g** tensor, this reflects the orientation-selected nature of the ENDOR technique. In the present study the ^{1,2}H pulsed ENDOR measurements also reflect the decomposition of the cluster EPR spectrum into contributions from two forms. For example, for $g \lesssim 2.016$, the EPR signal arises from the form 2 cluster, whereas for $g \gtrsim 2.029$ the form 1 signal dominates. Therefore, an ENDOR response at $g \lesssim 2.016$ can be assigned to the form 2 cluster and that at $g \gtrsim 2.029$ to the form 1 cluster. Signals in the intermediate region, $2.016 \lesssim g \lesssim 2.019$ might be expected to have contributions from both of the EPR-active components, although in general the form 1 signal is larger and will dominate.

Effects of Fe–Fe Spin-Coupling on Hyperfine Parameters. One can characterize an atomic site in a spin-coupled cluster by analyzing the observed hyperfine coupling to that site in terms of the intrinsic hyperfine constants that describe the electron–nuclear interaction in the absence of electron-spin exchange coupling within the cluster. Consider a nucleus (j) that is associated exclusively with a single iron site i; for example j might be Fe(i) itself ($j = i$ = Fe), a constitutive proton of cysteine bound to that Fe, or the ^{1,2}H of a H-bond to that cysteinyl sulfur. The observed hyperfine interaction $A(j)$ is described by the following equation:[29]

$$A(j) = K(i)\alpha(j,i) \qquad (3)$$

where $a(j,i)$ represents the intrinsic hyperfine coupling of the nucleus j to spin density that originates with the paramagnetic iron ion (i). The $K(i)$ are spin-projection coefficients that are determined by the spin-coupling among the i = 1–3 iron ions of the cluster (Chart 1) and obey the relation $K(1) + K(2) + K(3) = 1$. In contrast, a bridging inorganic sulfide of the cluster or an exchangeable proton/deuteron H-bonded to such a sulfur would have simultaneous indirect interactions with two or more iron ions. In this case eq 3 may be generalized as

$$A(j) = \sum K(i)\alpha(j,i) \qquad (4)$$

and the sum runs over all iron sites directly linked to the sulfur.[20,30] The spin-projection coefficients can be obtained theoretically by solving equations generated by a spin-coupling model for the [3Fe–4S]+ cluster[29] or can be estimated experimentally from observed iron hyperfine coupling constants through the use of eq 3. Mössbauer studies of [3Fe–4S]1+ clusters[22,29] yield representative[31] values for the isotropic hyperfine couplings of the three Fe ions of A(Fe(i)) = –44, 20, 3.4 MHz, i = 1–3. As the reference hyperfine coupling for an uncoupled, rubredoxin-like, tetrahedral Fe(III) ion with sulfur coordination, we take a(Fe,Fe) = –20.6 MHz.[33] Then eq 3 gives K(1) = 2.14, K(2) = –0.97, and K(3) = –0.17. These are collected in Table 1.

As before,[34] to proceed, we make the simplifying assumption that a proton H-bonded to a bridging sulfur experiences roughly the same intrinsic coupling to each iron bound to that sulfur, namely, $a(j,i) \approx a(j)$ in eq 4. This appears to be particularly

Chart 1

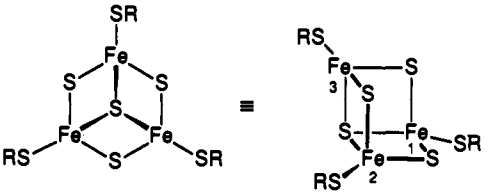

Table 1. Possible Binding Modes of Exchangeable Protons H1, H2, and H3 to the [3Fe–4S]+ Cluster in *D. gigas* Hydrogenase[a]

		binding modes[d]			
site of interaction[b]	K_{eff}[c]	1	2	3	4
Cys(1)	2.14				
Cys(2)	–0.97	H	H	H	
Cys(3)	–0.17				
S(1,2)	1.17	H	H		H
S(2,3)	–1.14	H		H	H
S(1,3)	1.97				
S(1,2,3)	1		H	H	H

[a] The hyperfine couplings for H1-H3 are given in Table 2. [b] The sulfurs are designated as a cysteinyl sulfur coordinated to Fe(i), i = 1–3, as a sulfide bridging two iron sites (i,j), or as the unique sulfide bridging all three Fe ions. [c] The coefficients for Cys(i), i = 1–3, are calculated from eq 3 using A(Fei) = –44, 20, 3.4 and a(Fe,Fe) = –20.6, as discussed in the text and ref 31. The vector coupling coefficient K_{eff} for the inorganic sulfides is defined in eqs 3 and 4a. [d] The data in Table 2, together with eqs 3 and 4a, indicate that $|K_{eff}| \sim 1$ for H1-H3. The Mims ^{2}H–^{2}H TRIPLE experiment shows that the hyperfine couplings of H1 and H2 are of opposite sign. Thus H1 and H2 must be assigned to sites whose K_{eff} are of comparable magnitude but opposite sign.

(28) Cammack, R.; Fernandez, V. M.; Schneider, K. In *Bioinorganic Chemistry of Nickel*; Lancaster, J. R., Jr., Ed.; VCH Publishers: Deerfield Beach, FL, 1988; pp 167–189.
(29) Kent, T. A.; Huynh, B. H.; Münck, E. *Proc. Natl. Acad. Sci. U. S. A.* **1980**, *77* (11), 6574–6576.
(30) Werst, M. M.; Kennedy, M. C.; Houseman, A. L. P.; Beinert, H.; Hoffman, B. M. *Biochemistry* **1990**, *29* (46), 10533–10540.
(31) We take A(Fe1) from the data for *D. gigas* hydrogenase (ref 22), but because the data for Fe2 and Fe3 is compromised by signals from [4Fe–4S] centers, we take A(Fe2) and A(Fe3) from the data for the [3Fe–4S]+ cluster of *A. vinelandii* ferredoxin II (ref 32).
(32) Emptage, M. H.; Kent, T. A.; Huynh, B. H.; Rawlings, J.; Orme-Johnson, W. H.; Münck, E. *J. Biol. Chem.* **1980**, *255*, 1793–1796.
(33) This value is close to a(Fe,Fe) = –20 MHz taken by Kent *et al.*, 1980 (ref 29). The value we chose is arrived at by requiring that $\sum_i K(i) = 1$, which would hold for spin-coupling within a cluster where all spin is localized on Fe. Delocalization would reduce $\sum K(i)$. Indeed, for the A(Fei) used by Kent *et al.* (ref 29), a(Fe,Fe) = –20 MHz yields $\sum_i K(i) = 0.9$. The arguments in the present paper are not altered by modifying the choice of the A(Fei) (ref 31) or a(Fe,Fe) within the ranges observed for these quantities.
(34) Houseman, A. L. P.; Oh, B.-H.; Kennedy, M. C.; Fan, C.; Werst, M. M.; Beinert, H.; Markley, J. L.; Hoffman, B. M. *Biochemistry* **1992**, *31* (7), 2073–2080.

reasonable for an oxidized [3Fe–4S]$^+$ cluster because all iron ions are in the same (ferric) oxidation state. In this case eq 4 simplifies to

$$A(j) = [\sum K(i)]\alpha(j) \equiv K_{eff}(j)\alpha(j) \quad (4a)$$

The K_{eff} for the three doubly-bridging S^{2-} and the triply-bridging S^{2-} are also presented in Table 1; the entries for S^{-2} are labelled by the indices of the Fe ions they bridge (Chart 1). Note that for an H-bond to a cysteinyl sulfur at site i, eqs 3 and 4a are the same, with $K_{eff}(i) = K(i)$, as the interaction is only to one Fe. The signs *and* magnitudes of the observed couplings are determined by the spin-projection coefficient. Simple spin delocalization from a cluster ferric ion to the exchangeable proton would lead to a positive $a(j)$, in which case the $A(j)$ coupling constants take the sign of the K_{eff}.

Field-Dependence of ^{1,2}H Pulsed ENDOR Signals. To fully characterize the bonding to the cluster, ^{1}H nuclear hyperfine interaction tensors were derived from Davies pulsed ^{1}H ENDOR spectra collected at numerous magnetic field positions across the EPR absorption envelope ($1.994 \leq g_{obs} \leq 2.022$) of hydrogenase samples in both H_2O (sample 3Fe–H) and D_2O (sample 3Fe–D). The bonding between an Fe ion of the [3Fe–4S]$^+$ cluster and its coordinated cysteinyl residue (Chart 1) can be studied by analyzing ^{1}H spectra of sample 3Fe–D, where all exchangeable protons have been replaced with deuterons. The only signals that remain are from constitutive ^{1}H, of which the β-CH_2 have the largest hyperfine coupling. Protons that are H-bonded to sulfur of the [3Fe–4S]$^+$ cluster are exchangeable, and their signals can be examined without interference from the constitutive protons in ^{1}H difference spectra (denoted $\Delta(^1H)$) from samples in H_2O (sample 3Fe–H) and D_2O (sample 3Fe–D) and in ^{2}H spectra of the deuterons introduced by exchange in the sample in D_2O.

Figures 3–6 each presents a set of these four types of spectra collected at a selected g value. A complete set of 11 spectra of each type is presented in the supplementary material, Figures S1–S4. The ^{2}H spectra are plotted with the x-axes scaled by the ratio $g_H/g_D = 6.514$. Thus, ^{1}H and ^{2}H splittings are directly comparable, and the spectrum of exchangeable deuterons can be matched to those of exchangeable protons (eq 2). The pulse width ($\pi/2$) employed was $t_p = 64$ ns for the Mims as well as the Davies spectra. This excites the electron spins within a width of *ca.* 5 G, which is a large fraction of the total width of the form 1 EPR signal (~30 G). Therefore, the ENDOR spectra presented here show a reduced orientation selection except at the two extreme edges of the EPR envelope. Lengthening the pulse to improve orientation selection would have reduced the sensitivity of the ENDOR measurement substantially.

Figure 3 displays single-crystal-like spectra taken at the low-field (g_1) edge of the EPR signal that is associated with form 1 only (Figure 2). Figure 4 comes from the maximum of the EPR spectrum where $g = g_2(1)$; both forms contribute, but form 1 dominates. Figure 5 is taken toward the high-field edge of the main EPR feature. This field is a single-crystal-like g_3 spectrum for form 1, although it has a contribution from $g \sim g_2$ for form 2. Finally, the spectra in Figure 6 were taken with the field set to the extreme high-field shoulder of the EPR spectrum, which is associated with form 2 only.

For the sample in H_2O there are numerous resolved ENDOR features at all field positions. The breadth of the ENDOR pattern is at least 8 MHz at all fields, but the largest coupling (~10 MHz) is seen at the low-field edge of the EPR envelope. Changes seen in the ENDOR spectra as the field is varied within the main EPR envelope are associated with orientation selection. This occurs for form 1 because its **g** tensor is well-defined.[7] At $g \sim g_3(1)$ (Figure 5), resolved peaks with narrow line widths are evident in spectra with contributions from exchangeable protons (all but the 3Fe–D spectrum). As these peaks are not seen in spectra

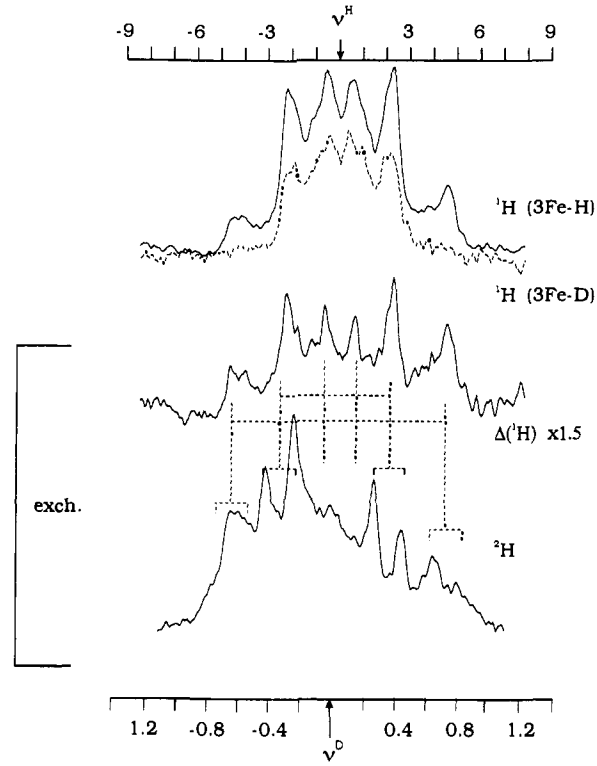

Figure 3. ^{1}H Davies and ^{2}H Mims ENDOR spectra of the [3Fe–4S]$^+$ cluster of *D. gigas* hydrogenase in H_2O (3Fe–H) and D_2O (3Fe–D) at $g = 2.032$, the low-field edge of the EPR envelope. (top) ^{1}H Davies ENDOR spectra of 3Fe–H (—) and 3Fe–D (- - -). The spectra are plotted as percentage ENDOR effect versus frequency offset from nuclear Larmor frequency (in MHz). The x-axis of the ^{2}H ENDOR is scaled up by a factor of 6.51 (eq 2). (middle) Percentage ENDOR effect difference spectrum. (bottom) ^{2}H Mims ENDOR. Three different classes of exchangeable proton resonances are assigned by hyperfine (|- - -|) and quadrupole splittings (—). Each spectrum consists of 256 frequency points. Conditions: Davies, 3Fe–H (9.5203 GHz, 0.3345 T), 64 ns $\pi/2$ microwave pulse, $\tau_{23} = 344$ ns, $t_{rf} = 20$ μs, rf power 350 W, 2 K, 10-Hz repetition rate, 96 transients. 3Fe–D (9.5101 GHz, 0.3341 T): 104 transients. All other conditions are the same as 3Fe–H. Mims (9.192 GHz, 0.3229 T): $\tau_{12} = 408$ ns, $t_{rf} = 35$ μs, rf power 200 W, 20-Hz repetition rate, 300 transients.

taken at fields 0.5 mT above and below this field, we can confidently assign this figure to a single-crystal-like spectrum at the high-field edge of form 1, confirming the decomposition of the EPR intensity. Above this field only form 2 contributes, and the frequencies of features in the spectra do not change with a change in g value. This implies the absence of an orientation-selection process within the high-field tail of form 2, as expected for spectra from a center sample whose **g** tensor exhibits a distribution of values; orientation selection is greatly suppressed for a distributed **g** tensor.[35] However, the features sharpen into peaks as the field is increased because a progressively narrower spread in g values for form 2 contributes to the ENDOR pattern. A relatively well-defined subset of the form 2 distribution is achieved by $g \sim g_3(2)$; Figure 6 presents the well-resolved ENDOR spectra collected there.

β-CH_2 Protons from Cysteine. As seen in Figures 3–6 (and S1–S4), the ^{1}H ENDOR spectra of the constitutive protons, as obtained from the hydrogenase in D_2O buffer (sample 3Fe–D), have lost most of the resolved structure seen with H_2O buffer. The relative ENDOR intensity, namely, the maximum percentage ENDOR effect, is between 4% and 5% for each spectrum, which is ~2/3 that exhibited by the protein in H_2O buffer (sample

(35) Houseman, A. L. P.; Doan, P. E.; Goodin, D. B.; Hoffman, B. M. *Biochemistry* **1993**, *32*, 4430–4443.

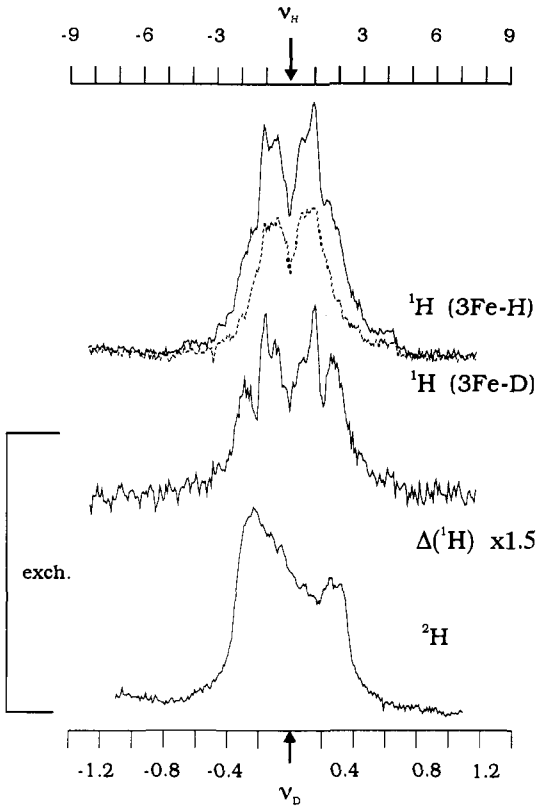

Figure 4. 1H and ^{2}H ENDOR spectra at $g = 2.022$, near maximum intensity of EPR signal. Conditions for Davies are same as Figure 3 except 3Fe–H (9.4656 GHz, 0.3345 T), 6-Hz repetition rate, 48 transients; 3Fe–D (9.4854 GHz, 0.3352 T). Conditions for Mims ENDOR: as Figure 3; 80 transients.

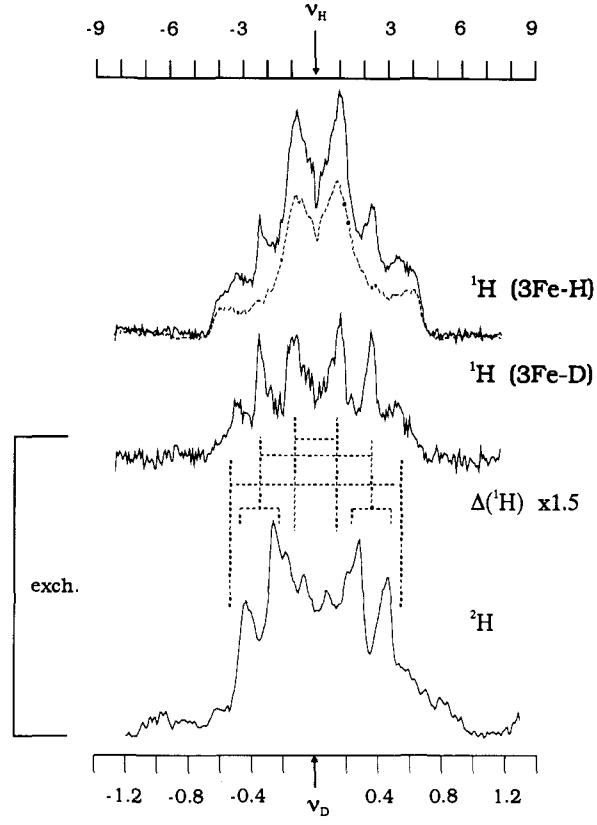

Figure 5. 1H and ^{2}H ENDOR spectra at $g = 2.016$, high field edge of form 1. Exchangeable resonances are assigned as in Figure 3. Davies ENDOR: conditions as in Figure 4 except 3Fe–H (9.4712 GHz, 0.3358 T), 3Fe–D (9.4854 GHz, 0.3362 T). Mims ENDOR (9.192 GHz, 0.3258 T): 200 transients.

3Fe–H). The breadth of the constitutive-proton ENDOR pattern of 3Fe–D is narrowest, 5 MHz, at the low-field edge of the EPR envelope (3325 G) (Figure 3). This single-crystal-like spectrum is solely associated with g_1 of form 1. Its breadth is determined by a well-resolved hyperfine-split doublet with $A_1(^1\text{Ha}) \approx 4$ MHz; closer inspection shows that this doublet in fact consists of two hyperfine-split doublets with slightly different couplings, A_1(Ha) $\sim$ 3.8, 4.2 MHz. The β-CH_2 protons of the three cysteines bound to the [3Fe–4S]$^+$ cluster are expected to have comparable *intrinsic* hyperfine coupling tensors.[20,36] Thus, from eq 3 one can confidently assign the Ha doublets to the β-CH_2 protons of cysteine bound to the iron ion with the largest vector-coupling coefficient, Fe(1) (Table 1). The inner doublet with $A_1(^1\text{H}) \lesssim 2$ MHz shows poorly resolved structure. It is assigned to overlapping resonances from the cysteines bound to Fe(2) and Fe(3): in particular, the β-CH_2 associated with Fe(3) are expected to have small values of A(H) because $K(3)$ is small (eq 3; Table 1).

As the field is increased from $g \sim g_1(1)$ (Figure 3) to $g \sim g_2(1)$ (Figure 4) and then to $g \sim g_3(1)$ (Figure 5), hyperfine anisotropy causes the ^{1}Ha resonances to spread smoothly to a larger coupling; by $g_3(1)$, the high-field edge of the form 1 EPR signal, this coupling reaches its maximum value of $A_3(^1\text{Ha}) \sim$ 7–8 MHz (Figure 5). As the pattern spreads, its broadest feature decreases in *relative* intensity; the major ^{1}Ha intensity shifts to a smaller splitting of $|A_2| \lesssim 2$ MHz at $g_2(1)$ and increases in *absolute* intensity. The mathematics of orientation selection require that the majority of the ENDOR intensity near g_2 is associated with the hyperfine tensor projection in the g_2 direction.[10] Thus, the field dependence of the spectra requires that $|A_2(^1\text{Ha})| < 2$ MHz; it suggests that $0 \lesssim A_2(^1\text{Ha}) < 2$ MHz. The field dependence of the ^{1}Ha frequencies *and* intensities further requires that $A_1(^1\text{Ha})$ and $A_3(^1\text{Ha})$ have the same sign, arbitrarily taken here to be positive (see below for a discussion of signs). The superposition of resonances from several different protons precludes accurate fitting of this data to obtain full hyperfine tensor components and orientations, as has been done in other instances.[8] However, the spectra from the constitutive β-CH_2 protons at fields associated with the three canonical g values show that the observed hyperfine tensor for the Ha protons from cys(a) has projections along the **g** tensor axes of $\mathbf{A}(^1\text{Ha}) \sim$ [4, (–2)–2, 7] MHz. This in turn allows us to calculate an apparent isotropic coupling of $A(^1\text{Ha}) \sim$ 3–4 MHz,[37] which corresponds to an *intrinsic* coupling of $a(^1\text{Ha}) \sim 1.3 - \sim 1.9$ MHz through eq 4a. Likewise, through eqs 3 and 4a, the observed couplings for the β-CH_2 constitutive protons from the other two cysteines appear to be consistent with intrinsic couplings in this range (Table 2).

As the field is increased further, into the "tail" of the EPR spectrum, form 1 no longer contributes (Figure 1). The breadth of the ENDOR spectrum seen throughout the form 2 tail is approximately the same as that for form 1 at $g_3(1)$, but the resolution at first is low. It becomes increasingly better as the field is raised because only at the highest fields (Figure 6) does a relatively well-defined subset of form 2 molecules contribute to give a well-resolved single-crystal-like ENDOR spectrum.[35] Here the overall pattern is similar to that at $g_3(1)$, but we now can even more clearly identify three doublets from the three cysteines bound to the cluster, with hyperfine couplings of $\sim$1, 2, and 7 MHz. The similarity of the 3Fe–D ^{1}H spectra for forms 1 (Figure 5) and 2 (Figure 6) indicates that the hyperfine couplings to the β-CH_2 of forms 1 and 2 are essentially the same; as a result, the values listed in Table 2 for $A_3(^1\text{H})$ of ^{1}Hb and ^{1}Hc are those from form 2.

(36) Mouesca, J.-M.; Rius, G.; Lamotte, B. *J. Am. Chem. Soc.* **1993**, *115*, 4714–4731.

(37) We note that $A = \text{Tr}(\mathbf{A})/3$. As Tr(**A**) is invariant to rotations of the hyperfine tensor, to compute A, we only need the values along the **g** tensor axes.

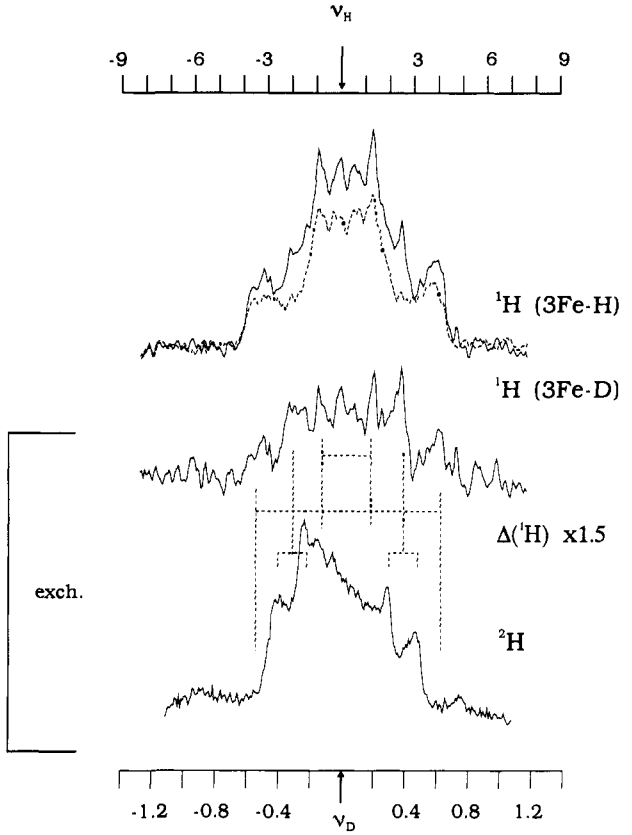

Figure 6. ^{1}H and ^{2}H ENDOR spectra taken at $g = 2.004$ in the form 2 tail of the EPR envelope. Exchangeable resonances are assigned as in Figure 3. Conditions are the same as Figure 3 except Davies 3Fe–H (9.5203 GHz, 0.3390 T), 128 transients, 3Fe–D (9.5101 GHz, 0.3390 T), 168 transients. Mims: 0.3273 T, 300 transients.

Table 2. Hyperfine and Quadrupole Coupling Constants (MHz) for Protons of the Form 1 $[3Fe\text{–}4S]^{1+}$ Cluster of *D. gigas* Hydrogenase

	A(^{1}H) [A_1, A_2, A_3; A; a][a]	P(^{2}H)
Cys(β-CH_2) Protons[b]		
Ha	[4[c], (−1)–(+2), 7–8; ~3–4; ~1.4–1.9]	
Hb	[1, ≤2, ~2.5[d,e]; 1–2; ~1–2]	
Hc	[<1, <2, ~1[d,f]; g; g]	
H-Bonded Protons[h]		
H1	±[9.2, ~1, 2; ~4; ~4]	$P_1 \approx 0.06$
H2	∓[4.2, ~4, 5; ~4; ~4]	$P_1 \approx 0.06$
H3	[1.2, ~1, 7; ~3; ~3]	$P_3 \approx 0.06$

[a] The observed isotropic coupling is represented by A; the intrinsic coupling calculated according to eq 4a is a. [b] Protons Ha are on Cys bound to the unique iron ion Fe(1). Hb and Hc are assigned to Fe(2) and Fe(3). The signs of the constitutive proton tensors are not determined experimentally; according to eq 3, they all are positive. [c] The spectra actually show resolved couplings of 3.8 and 4.2 MHz, presumably from the two inequivalent β-CH_2 protons. [d] The g_3 spectra of β-CH_2 protons for forms 1 and 2 are similar, but at g_3 better resolved for form 2 (see text). Thus, the values of A_3 for form 2 are included in the table. The spectra further resolve two couplings, presumably from the two inequivalent β-CH_2 protons. [e] The two resolved couplings are $A_3 = 2.4, 2.6$ MHz. [f] The two resolved couplings are $A_3 = 0.9, 1.1$ MHz. [g] The poor resolution of the small observed coupling does not warrant an estimate. [h] ^{2}H–^{2}H Mims TRIPLE resonance shows that A(H1) and A(H2) have opposite signs; the sign of A(H3) is not determined experimentally. Form 2 also displays resonances from three strongly-coupled exchangeable H-bonds at $g_3(2)$. Their A_3 values correspond to those for form 1. See text.

H-Bonded Protons. The effects of H/D exchange in the single-crystal-like ENDOR spectra from form 1 taken at the low field edge, $g_1(1)$, of the EPR envelope are seen to extend across the entire width of the ^{1}H and ^{2}H spectra (Figure 3). The Δ(^{1}H) H/D difference spectrum shows distinct resonances from three strongly-coupled exchangeable protons: a fairly broad hyperfine-split doublet with $A_1(^1H1) = 9$ MHz and sharper doublets with $A_1(^1H2) = 4$ MHz and $A_1(^1H3) = 2$ MHz. Consideration of the intensities of these resonances, along with their field dependence (see below) indicates that H1 and H2 are each associated with a single proton; we treat H3 as the same, although here the data is not as conclusive. Additional intensity is seen for more weakly coupled exchangeable protons; no detailed analysis is possible for these. The ^{2}H resonances in Figure 3 show peaks that correspond to those from H1 and H2. Each has a resolved quadrupole splitting of $3P(^2H) = 0.20$ MHz, values consistent with those expected for a H-bonded deuteron.[38] The ^{2}H peaks from H3 are unresolved.

In the spectra at the maximum of the EPR envelope, near $g \sim g_2(2)$ (Figure 4), the Δ(^{1}H) and ^{2}H spectra "collapse" and show their minimal breadth, with all resonances falling in a range $\nu_H \pm 2$ MHz, corresponding to $|A(^1H)| \lesssim 4$ MHz. As the field is further increased, the Δ(^{1}H) and ^{2}H patterns again broaden and sharpen until they reach the high-field edge of the form 1 EPR spectrum (Figure 5). Here there are again resolved doublets from three exchangeable protons, H1′, H2′, H3′, with proton couplings of $A_3(^1H) \sim 7$, 5, and 2 MHz, respectively. The ^{2}H spectrum shows a sharp quadrupole-split doublet from ^{2}H2′, with $3P(^2H2') \approx 0.2$ MHz. The Δ(^{1}H) signal from ^{1}H1′ is broad, and the corresponding ^{2}H1′ signal is further smeared by quadrupole couplings. Finally, there is additional intensity near ν_D from ^{2}H3′ and perhaps other unresolved deuterons. Careful consideration of the full field dependence of the Δ(^{1}H) spectra (Figure S3) shows that H1′ observed at the high-field edge of form 1 does *not* correlate with the strongly-coupled H1 seen at the low-field edge. Thus, H1 has a large coupling at low field (g_1) and smaller couplings at higher fields (g_2, g_3), with the converse being true for H2 or H3. Because of the spectral congestion, the hyperfine tensor for the three resolvable H-bonds cannot be determined precisely. Nonetheless, semiquantitative estimates for the tensors for H1 and H2 can be achieved from careful examination of the field dependencies, with the tensor for H3 being somewhat less certain (Table 2). These lead to estimates for the *intrinsic* isotropic couplings of $a(^1H) \sim 4$ MHz for H1 and H2 and $a(^1H3) \sim 3$ MHz.[37]

As the field is increased into the "tail" region, where only form 2 contributes (Figure 1), the excellent resolution in Figure 5 is immediately lost, as with the constitutive protons, because the g distribution leads to a distribution in contributing molecular orientations. At the high-field edge of the EPR tail the ^{1}H and Δ(^{1}H) signals sharpen because now only a well-defined set of molecules contributes those with the minimum value of g_1; however, the EPR signal and thus the absolute ENDOR response is greatly diminished and the S/N of the Δ(^{1}H) signal is poor (Figure 6). Nonetheless, it is possible to resolve doublets from three exchangeable protons in the Δ(^{1}H) spectrum, with $A_3(^1H) \approx 7$, 5, and 2 MHz. This agrees well with the observations at the high-field edge for form 1. The ^{2}H spectrum shows a quadrupole-split doublet from ^{2}H2′ with $3P(^2H2') \approx 0.25$ and $A(^2H)$ corresponding to $A(^1H2') \sim 5$ MHz, again as seen with form 1.

Because the EPR spectrum of form 2 is weaker than and largely overlapped with that of form 1, it is impossible to characterize the exchangeable protons from form 2 at any field other than the high-field edge of the spectrum. Nonetheless, comparison of the corresponding edge spectra for form 1, Figure 5, and form 2, Figure 6, clearly suggests that the three principal hyperfine values for the strongly-coupled H-bonded proton are quite comparable in the two forms.

^{2}H–^{2}H Mims TRIPLE-resonance. A ^{2}H–^{2}H "general" TRIPLE-resonance measurement[2,3,5] was performed on the hydrogen-bonded deuterons of sample 3Fe–D. This experiment correlates the properties of signals from two different nuclei. It can

(38) Edmonds, D. T. *Phys. Rep.* **1974**, *29* (A), 233.

determine (i) whether they are associated with the same spin system, namely, with the same orientation of a single cluster form and (ii) the relative signs of their hyperfine coupling. The technique involves the application of two rf fields to ENDOR transitions of the two nuclei. A fixed "pump" frequency is applied to a selected transition of one nucleus; a second frequency is swept through the spectrum to "probe" other nuclei. If the pumped nucleus and a probed nucleus are associated with *different* electron spin systems, then only the ordinary ENDOR spectrum of the probed nucleus is seen in the presence of the pump; the difference TRIPLE spectrum, [pump on – pump off], is featureless. If, however, the two nuclei are part of the *same* spin system, the pump pulse causes a change in the intensity of the probe nucleus's ENDOR signal, leading to a peak in the *difference* TRIPLE spectrum. Thus, if two deuterons introduced by H/D exchange give a ^{2}H–^{2}H TRIPLE-resonance response at a single-crystal-like field value, the two *must* be associated with the same cluster form. The sign of the resulting difference TRIPLE signal further gives the relative signs of the hyperfine couplings of the pumped and probed nuclei. For example, tuning the pump frequency to a $\nu_{\mp}$ transition of nucleus i will give a positive difference TRIPLE signal when probing a $\nu_{\pm}$ transition of nucleus j when $A(i)$ and $A(j)$ have opposite signs and *vice versa*.

Mims ^{2}H–^{2}H difference TRIPLE-resonance spectra were obtained at the extreme low-field edge of the EPR signal where the well-defined single-crystal-like spectra of Figure 3 were collected. At any other field, multiple orientations contribute to the EPR signal. Because of the anisotropy in hyperfine and quadrupole coupling constants, each pump frequency excites a range of different molecules with differing TRIPLE spectra, distributing the effects. The situation is even more complicated for ^{1}H TRIPLE because a signal at any field position would be the net response from the overlapping exchangeable and non-exchangeable protons, which may or may not have the same sign of their coupling constants. Thus, predictably, attempts to perform ^{1}H–^{1}H TRIPLE, even at the low-field edge of the spectrum, were unsuccessful.

Figure 7A reproduces the low-field single-crystal-like ^{2}H ENDOR spectrum, and Figure 7B is a ^{2}H–^{2}H difference TRIPLE spectrum obtained by pumping the $\nu_-(m)$ ENDOR line of ^{2}H1 at $\delta\nu_-^D = -0.63$ MHz (Figure 7A). It consists of a spike (which carries no information) at the pumping frequency $\delta\nu_-^D = -0.63$ MHz and two *positive* peaks at $\delta\nu_+^D = 0.26$ and 0.43 MHz, which correspond to the $\nu_+(m)$ transitions of ^{2}H2. This is a TRIPLE response, not simply a portion of an ordinary ^{2}H2 ENDOR pattern, because it is observed in the difference spectrum and because the $\nu_-(m)$ peaks are not similarly enhanced. Likewise, pumping on the $\nu_+(m)$ ENDOR line of ^{2}H1 at $\delta\nu_+^D = +0.63$ MHz gives a mirror-image spectrum (Figure 7C) with a spike at the pumping frequency and two *positive* peaks at $\delta\nu_-^D = -0.26$ and -0.43 MHz, the $\nu_-(m)$ lines of ^{2}H2. Pumping on the transition of ^{2}H2 gives equivalent TRIPLE responses from ^{2}H1, although they are more difficult to observe because the ^{2}H1 signals are intrinsically weaker at any single frequency due to the increased line width seen in the ^{1}H ENDOR pattern.

The observation of the difference TRIPLE spectrum correlating ^{2}H1 and ^{2}H2 indicates that they are indeed associated with the same [3Fe–4S]$^+$ paramagnetic center. This measurement thus confirms the EPR decomposition that assigns the EPR intensity at this field entirely to form 1. Because pumping on the $\nu_{\mp}$ transition of the ^{2}H1 signal gives a positive response in $\nu_{\pm}$ transition of the ^{2}H2 signal, the hyperfine coupling constants $|A(^2\text{H1})| = 1.4$ MHz and $|A(^2\text{H2})| = 0.7$ MHz must have *opposite* signs;[3,39] by eq 2; the same of course is true for the ^{1}H coupling constants.

Sites of H-Bond Interactions. There are *a priori* $N = 7 \times 6 \times 5/3! = 35$ ways in which the three strongly-coupled H-bonded protons, H1, H2, and H3, *might* be distributed over the four bridging and three mercaptide sulfurs of the [3Fe–4S]$^+$ cluster (Chart 1), assuming one interaction/ligand; there are additional possibilities if 2:1 interactions are considered. However, if H1 and H2 were bonded to the [3Fe–4S]$^+$ cluster at the same cysteine or through the same bridging sulfur, they would share the same coefficient $K(i)$ and hence have the same signs for the hyperfine coupling constants. The ^{2}H TRIPLE spectra show that this is *not* the case. Therefore, these two exchangeable protons necessarily are H-bonded to different sulfurs. As H1 and H2 have comparable observed isotropic hyperfine couplings, A(H), then according to eq 4a, they are likely to be associated with sites whose K_{eff} are of comparable magnitude, but of opposite sign. The K_{eff} for H3 is likely to have a similar magnitude; its relative sign is not determined. These conditions are met if the H-bonds are distributed among the four sites listed in Table 1, Cys(2), S(2,3), S(1,2), and S(1,2,3); all have $|K_{\text{eff}}| \sim 1$, with the first two being negative. This eliminates Cys(1), Cys(3), and S(1,3). As we do not know the sign of A(H3), there are four binding modes with one H-bond/site that appear to satisfy these constraints (Table 1). Each of these modes is obviously associated with several others in which two protons with hyperfine couplings of the same sign, H1 and H3 or H2 and H3, interact with a single site. Given the assignment of H-bonds to sulfur sites having $|K_{\text{eff}}| \sim 1$, then $A(\text{H}) \sim a(\text{H})$, which leads us to conclude that each of the three well-resolved H-bonds has an intrinsic coupling constant of $a(^1\text{H}) \sim 3$–4 MHz (Table 2).

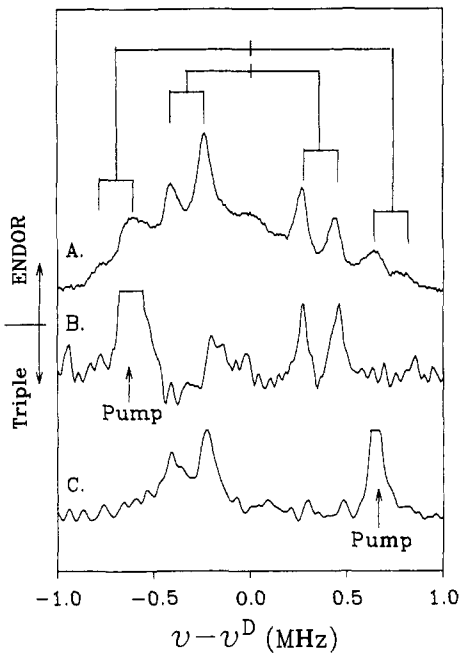

Figure 7. Mims ^{2}H pulsed ENDOR and ^{2}H–^{2}H TRIPLE-resonance spectra of *D. gigas* hydrogenase [3Fe–4S]$^+$ cluster taken at the low-field edge of EPR absorption envelope. (A) same spectrum as Figure 6D; (B, C) difference TRIPLE spectra with pump frequency set to $\delta\nu_D = -0.63$ MHz (B) and +0.63 MHz (C). Experimental conditions for B and C: microwave frequency 9.20 GHz, $B_0 = 3229$ G, $t_p = 64$ ns, $\tau = 404$ ns, $t_{rf}(p) = t_{rf}(s) = 55$ μs, pump frequency 1.48 MHz (B), 2.74 MHz (C).

Discussion

Our combined pulsed ^{1,2}H ENDOR and ^{2}H–^{2}H Mims TRIPLE resonance studies have allowed us to characterize the constitutive cysteinyl β-CH_2 as well as the H-bonding protons associated with the *D. gigas* hydrogenase [3Fe–4S]$^+$ cluster. One immediate result of these measurements is the confirmation that the cluster adopts a bimodal distribution of conformational forms or

(39) Kevan, L., Bowman, M., Eds. *Modern Pulsed and Continuous-Wave Electron Spin Resonance*; Wiley: New York, 1990; p 195.

substates.[40] Our previous conclusion that cluster form 1 is structurally well-defined was based on its well-defined **g** tensor and the orientation-selective ^{57}Fe ENDOR of Fe(1).[7] This conclusion now is confirmed by the ^{1,2}H orientation-selective ENDOR from both constitutive and H-bonded protons. In contrast, form 2 comprises a set of substates with different properties, including a distribution in **g** tensor values and a resultant loss of ENDOR orientation selection. The ^{1,2}H ENDOR does not, however, disclose any obvious features that could be the basis for the structural differences between the two cluster forms.

The ^{1}H ENDOR of the β-CH_2 protons of the cysteines bound to the ferric ions of the cluster in form 1 have intrinsic isotropic couplings that *must* fall in the range $1.3 \leq a(H) < 1.9$ MHz; in particular, the two Ha protons of the cysteine attached to Fe1 appear to have comparable couplings that are within this range. These conclusions are quite consistent with and supportive of recent results from single-crystal ENDOR studies of a [4Fe–4S]$^{3+}$ model compound by Mouesca *et al.*[36] In this elegant work it was proposed that the intrinsic isotropic coupling for a β-CH_2 proton of cysteine bound to Fe of an [*n*Fe–*m*S] cluster can be described to a good approximation by a general function of the dihedral angle (θ) between the Fe–S–C and S–C–H planes. We choose to write their function as

$$\alpha = A + B\cos(\theta + \theta_0) - C\cos^2(\theta + \theta_0) \qquad (5)$$

where they have determined that[41] $A \approx 3$, $B \approx 0.5$, $C \approx 2.3$ MHz, and $\theta_0 \approx -20°$. As the initial attempt to correlate the present results with those on the model, we idealize the Ha couplings as being identical and take the geometry at the β-CH_2 such that one H has a dihedral angle θ and the other has $\theta \pm 120°$. Then according to eq 5, there are several values of θ for which the β-CH_2 protons have equal couplings. Two of these give $a \approx$ 1.3–1.6 MHz,[41] which is within the range we have proposed for the Ha protons and corresponds to a Fe–S–Cβ–Cα dihedral angles of $\sim$280° and $\sim$120°. Both angles are similar to values exhibited by cysteine in ferredoxins, with the former falling in a particularly common range.[18]

These results provide an important bridge between low-temperature ^{1,2}H pulsed ENDOR measurements and solution-NMR studies of cluster structure. Solution-NMR studies of the contact-shifted resonances associated with an [*n*Fe–*m*S] cluster give detailed information about the structure of the cluster cysteinyl ligands[42] *and* about the cluster's electronic structure. The latter can be obtained by analyzing the contact shift of a nucleus coupled to one or more of the Fe ions in terms of the thermal populations of the full set of spin multiplets for the spin-coupled cluster.[19-21] If the values of the intrinsic hyperfine couplings, $a(j,i)$ (eq 4), are known, the contact shifts measured by NMR can be used to deduce the exchange interaction parameters that determine the multiplet energies through the Heisenberg–Dirac–Van Vleck spin exchange among the iron ions of an [*n*Fe–*m*S]$^+$ cluster.

The arbitrary choice of $a = 1$ MHz for all cysteinyl β-CH_2 has been adopted in a number of studies,[20] in particular that on the [3Fe–4S]$^+$ cluster of *D. gigas* FdII.[21] The protein and model ENDOR measurements confirm that $a = 1$ MHz is a reasonable guess, but is somewhat low. Our data indicate values of a that are $\sim$30–100% greater, and Mouesca *et al.*[36] indicate that these values can be as much as 3-fold greater. We thus provisionally propose that a conservative minimum value, $a \sim 1.5$ MHz, be adopted in the absence of direct ENDOR measurements on the protein of interest. In some instances, at least, use of the larger a could have significant effects on the exchange parameters calculated from observed shifts or on shifts predicted from known or assumed couplings. The results presented here suggest that pulsed ^{1,2}H ENDOR on [*n*Fe–*m*S]$^+$ clusters will be of greatest value in studying the bonding to those Fe sites of a cluster that have the largest spin-projection coefficients and thus the largest observed hyperfine interaction.

The third and central result of our study is a characterization of three NH···S hydrogen bonds with well-resolved hyperfine interaction, each with intrinsic isotropic couplings of $a \sim$ 3–4 MHz, 2–3-fold *larger* than those to the β-CH_2. With the knowledge of the relative signs of the hyperfine tensors for H1 and H2, as determined by Mims ^{2}H–^{2}H TRIPLE and the use of eqs 3 and 4, we inferred that H1, H2, and likely H3 form an H-bond to one of the four sulfur sites listed in Table 1. However, one of these sites is the triply-bridging sulfur, S(1,2,3) (Chart 1). Crystal structures have been determined for several proteins with [3Fe–4S] clusters, and thus even without structural data for the *D. gigas* hydrogenase there is information regarding H-bonding patterns for such clusters. For the [3Fe–4S]$^+$ cluster of *D. gigas* FdII[15] the three doubly-bridging S^{2-} ions and two of the cysteinyl-sulfur ligands appear to be involved in a total of eight NH···S hydrogen bonds with backbone amides, whereas the triply-bridging S^{2-} is located in a non-polar environment and is *not* H-bonded. The [3Fe–4S] of *A. vinelandii* FdI shows an analogous pattern of H-bonding, with as many as a total of seven (depending on the assumed cutoff distance) NH···S hydrogen bonds involving the three doubly-bridging S^{2-} and two of the three cysteinyl-sulfurs, but *none* to the trivalent sulfur.[14,16] Likewise, there are *no* H-bonds to the trivalent sulfur of the aconitase [3Fe–4S]$^+$ cluster[43] *nor* to the corresponding sulfur of the four-iron cluster of *Peptococcus aerogenes* (now *Peptostreptococcus asaccharolyticus*) ferredoxin.[18] By analogy, we take the same to hold here. In this case the candidates for acceptors of the strong H-bond are the sulfur of Cys(2) and the divalent sulfides, S(1,2) and S(2,3); the binding modes 2–4 of Table 1 for the [3Fe–4S]$^+$ cluster of hydrogenase are eliminated. From examination of Table 1, the only one of these candidates with $|K_{eff}| \sim 1$ and $K_{eff} > 0$ is S(1,2). Thus, the ENDOR constraint that both positive and negative values of K_{eff} are involved requires that the H-bond pattern includes one to S(1,2). If there is one interaction per site, the indicated pattern is binding mode 1, where the strongly-coupled H-bonds are to the sulfur of Cys(2) and to divalent sulfides S(1,2) and S(2,3). With two interactions per site, then the indicated sites of the strong H-bonding are S(1,2) and either Cys(2) *or* S(2,3). In any case, the pattern of strong H-bonds appears to be quite unsymmetric, involving only one face of the cluster (Figure 8). Applications of this approach to clusters of known X-ray structure will provide a test of the simplifying assumption that led to eq 4a, and thereby to the site assignments.

It has been suggested that H-bonding to the sulfur ligand of an [*n*Fe–*m*S] cluster might serve to tune its redox potential and might even serve to select an individual Fe site in a valence-trapped system.[4,17,18] The large isotropic hyperfine couplings for the three H-bonds studied here imply a degree of covalency that might well impart a sufficient free energy of stabilization to serve in these roles.

The ENDOR data on the H-bonded protons again imply a connection to solution-NMR studies. Protons with large isotropic

(40) Frauenfelder, H.; Sligar, S. G.; Wolynes, P. G. *Science* **1991**, *254*, 1598–1603.

(41) The quantities (A, B, C) were calculated in Mouesca *et al.*, 1993 (ref 36), from experimental values of observed hyperfine couplings. They were related to the intrinsic couplings using a generalization of the $K(i)$, the spin populations, $D_S(i)$: $A = D_S a$, analogous to eq 3. The $D_S(i)$ were normalized to $\sum D_S(i) = 1.28$; as is noted there, the normalization should be 1.0. Indeed, $K(i)$ calculated there for the idealized spin-coupling model employed in eqs 3 and 4 are normalized to 1.2, not 1.0. Thus, the parameters A, B, C and the a calculated from eq 5 may be *under*estimated correspondingly.

(42) Dugad, L. B.; La Mar, G. N.; Banci, L.; Bertini, I. *Biochemistry* **1990**, *29* (9), 2263–2271.

(43) Robbins, A. H.; Stout, C. D. *Proteins: Struct., Funct., Genet.* **1989**, *5*, 289–312.

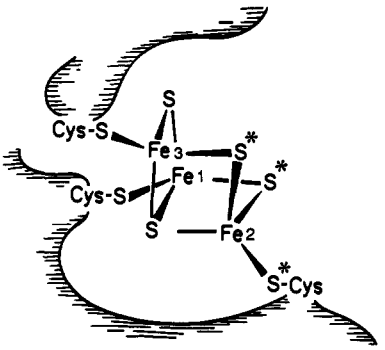

Figure 8. Representation of the [3Fe–4S]⁺ cluster as bound to the protein, with proposed H-bonding sites indicated by (asterisks).

couplings such as the hydrogen bonds H1-H3 exhibit correspondingly large solution-NMR chemical shifts, but unfortunately are typically associated with large NMR line width: they might easily be missed in ^{1}H NMR studies. On the other hand, the ^{1,2}H ENDOR spectra of exchangeable protons show signals from other H-bonded protons with couplings too small to be well-resolved in ENDOR; these are more readily studied by NMR. Thus, we envisage complementary and mutally supportive roles for these two methods.

Acknowledgment. We thank Mr. Clark E. Davoust for his assistance and Dr. A. L. P. Houseman for accumulating corroborative CW ^{1}H ENDOR spectra, and Dr. Joshua Telser for helpful discussions. We also thank Professors E. Adman and C. D. Stout for helpful discussions of X-ray diffraction results. The *D. gigas* hydrogenase samples were kindly provided by Professors Boi-Hanh Huynh and Jean Le Gall. This work has been supported by NIH HL 13531 and NSF MCB 9207974.

Supplementary Material Available: Four figures containing ^{1,2}H ENDOR spectra taken at multiple fields across the EPR envelope of the [3Fe–4S]⁺ cluster of *D. gigas* hydrogenase (5 pages). This material is contained in many libraries on microfiche, immediately follows this article in the microfilm version of the journal, and can be ordered from the ACS; see any current masthead page for ordering information.